Supramolecular Organization in Organic Inorganic Heterogeneous Hybrid Catalysts Formed from Polyoxometalate and Poly(ampholyte) Polymer

ARTICLE *in* LANGMUIR · MARCH 2013

Impact Factor: 4.46 · DOI: 10.1021/la400055t · Source: PubMed

6 AUTHORS, INCLUDING:

Gijo Raj
CEA
27 PUBLICATIONS **99** CITATIONS
SEE PROFILE

Alain Guillet
Université catholique de Louvain
10 PUBLICATIONS **87** CITATIONS
SEE PROFILE

Bernard Nysten
Université catholique de Louvain
187 PUBLICATIONS **3,332** CITATIONS
SEE PROFILE

Eric M. Gaigneaux
Université catholique de Louvain
219 PUBLICATIONS **2,757** CITATIONS
SEE PROFILE

Langmuir

Article

pubs.acs.org/Langmuir

Supramolecular Organization in Organic–Inorganic Heterogeneous Hybrid Catalysts Formed from Polyoxometalate and Poly(ampholyte) Polymer

Gijo Raj,*[,†] Colas Swalus,[†] Alain Guillet,[§] Michel Devillers,[†] Bernard Nysten,[‡] and Eric M. Gaigneaux*[,†]

[†]Institute of Condensed Matter and Nanosciences, Division Molecules, Solids and Reactivity, [‡]Division Bio and Soft Matter, and [§]Institute for Multidisciplinary Research in Quantitative Modelling and Analysis, Platform SMCS, Université catholique de Louvain, B-1348 Louvain-la-Neuve, Belgium

Supporting Information

ABSTRACT: Hybridization of polyoxometalates (POMs) via the formation of an organic–inorganic association constitutes a new route to develop a heterogeneous POM catalyst with tunable functionality imparted through supramolecular assembly. Herein, we report on strategies to obtain tunable well-defined supramolecular architectures of an organic–inorganic heterogeneous hybrid catalyst formed by the association of a hydrophobically substituted polyampholyte copolymer (poly *N, N*-diallyl-*N*-hexylamine-*alt*-maleic acid) and phosphotungstic acid ($H_3PW_{12}O_{40}$) POMs. The self-assembling property of the initial polyampholyte copolymer matrix is modulated by controlling the pH of the hybridization solution. When deposited on a mica surface, isolated, long and extended polymer chains are formed under basic conditions (pH 7.9), while globular or coiled structures are formed under acidic conditions (pH 2). The supramolecular assembly of the POM-polymer hybrid is found to be directed by the type and quantities of charges present on the polyampholyte copolymer, which themselves depend on the pH conditions. The hypothesis is that the Keggin type $[PW_{12}O_{40}]^{3-}$ anions, which have a size of ∼1 nm, electrostatically bind to the positive charge sites of the polymer backbone. The hybrid material stabilized at pH 5.3 consists of POM-decorated polymer chains. Statistical analysis of distances between pairs of POM entities show narrow density distributions, suggesting that POM entities are attached to the polymer chains with a high level of order. Conversely, under acidic conditions (pH 2), the hybrid shows the formation of a core–shell type of structure. The strategies reported here, to tune the supramolecular assembly of organic–inorganic hybrid materials, are highly valuable for the design and a more rational utilization of POM heterogeneous catalysts in several chemical transformations.

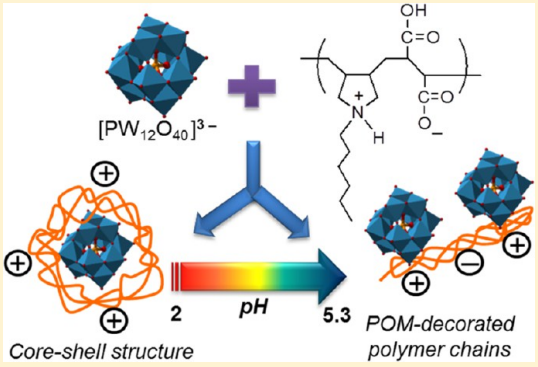

INTRODUCTION

Polyoxometalates (POMs) are well-defined anionic clusters of early transition-metal oxides and are currently a major area of research in inorganic chemistry.[1−3] Their tunable physicochemical properties, such as molecular architecture, surface charge densities, strong redox capability, and electro and photochemical properties, make these molecular metal-oxide nano clusters valuable in various fields such as magnetism,[4−6] electronics,[7] electro and photochromic systems,[8,9] medicine,[10] molecular batteries,[11] and catalysis.[12−15] In catalysis, POM exhibits high Brönsted acidity and very fast redox transformations under soft conditions, which enable them to be used as efficient acid or oxidation catalysts.[16]

Heterogenization of the POM anions in an organic matrix to create organic–inorganic hybrid catalysts is a recent trend in heterogeneous catalysis technology.[17,18] Hybridization of POM offers new routes to generate well-defined, functional molecular and supramolecular architectures either by covalent functionalization of POM with an organic species[19−21] or through the formation of organic-cation encapsulated systems driven by electrostatic interactions.[5,17,22] This later approach of hybridization through electrostatic interactions was recently reported to exhibit many advantages in a multitude of catalyst design. For example, Onmatsu et al.[23] have recently reported that ion-paired chiral ligands formed through electrostatic interactions rather than covalent bonding, achieve high enantioselectivity in palladium catalysis. Organic–inorganic hybridization through electrostatic interactions represents a means to confer POM increased functionalities, as well as an improved processability, avoiding deactivating covalent bonding with the active sites and preventing unavoidable leaching via simple physical blending.

Traditionally, cationic surfactant molecules [e.g., dimethyldioctadecylammonium bromide (DODA)] were employed to form surfactant-encapsulated clusters (SECs) of POM.[22,24,25] Direct imaging of these SECs by scanning probe microscopy techniques put forward molecular models in which the anionic

Received: January 7, 2013
Revised: March 8, 2013
Published: March 12, 2013

   dx.doi.org/10.1021/la400055t | *Langmuir* 2013, 29, 4388−4395

POM was surrounded by hydrophobic chains of cationic DODA.[24] Even though SECs represent a high level of self-assembly and host−guest interactions, an intriguing challenge, for a catalytic application, would be to achieve ordered hybrid structures with POM on surfaces, still keeping them readily accessible to the reactant molecules. POM hybrid structures with unfolded long-range ordered organic chains are thus targeted here. These are expected to have more valuable catalyst performances, since the active sites of POM would then not be trapped inside a hydrophobic shell.

Recently, zwitterionic poly(ampholyte) polymers resulting from the combination of monomers bearing carboxylic acid and amine moieties were shown to constitute an interesting system to develop organic−inorganic hybrid materials.[26,27] The structure of these polymers was designed to stabilize and interact with anions and cations of a dissolved inorganic salt by electrostatic interactions. Compared to surfactant molecules such as DODA, the poly(ampholyte) polymer offers additional advantages such as solubility in various polar media, and a high number of potential binding sites for each type of inorganic ion (both cations and anions). Such polymer systems have been used earlier to form hybrid organic−inorganic precursors in the preparation of mixed nickel and cobalt molybdates.[27,28] However, hybrid materials based on poly(ampholyte) polymers and POM were not yet explored, and the substantial challenge here is a clear understanding of the parameters that allow tuning the supramolecular architecture of the organic−inorganic hybrid, which in turn impacts the hybrid catalyst performance. In the family of POMs, phosphotungstic acid ($H_3PW_{12}O_{40}$) was extensively studied in catalysis reactions due to its high acid strength and high thermal stability.[29,30] Moreover, the organic−inorganic hybrid of phosphotungstic acid has received considerable interest in diverse fields such as polymer electrolyte fuel cells[31] and photochromism.[32] It is thus evident that $H_3PW_{12}O_{40}$ has unique and fascinating properties that have attracted extensive interest in several scientific domains.

Scanning probe microscopy has emerged as a powerful technique to characterize POM molecules, as well as organic−inorganic hybrid material, with nanometer or even subnanometer resolution.[19,24,33,34] Herein, we used atomic force microscope (AFM) to probe the supramolecular organization of an organic−inorganic hybrid formed from phosphotungstic acid, $H_3PW_{12}O_{40}$ and poly(*N*,*N*-diallyl-*N*-hexylamine-*alt*-maleic acid) polymer. The supramolecular organization of the poly(ampholyte) polymer matrix, which can be controlled via the pH conditions, is used here to direct the organization of POM anions that bind to the positively charged sites on the polymer chains through electrostatic interactions. Particularly, the use of the AFM HarmoniX imaging mode that enables simultaneous measurements of topography and nanomechanical properties, such as peak force, adhesion force, and elastic modulus, allows one to clearly distinguish, with high spatial resolution, the POM and polymer components in the hybrid film and thus provide new insights into the formation of organic−inorganic hybrid materials. This might lead toward a more rational design of hybrid organic−inorganic catalysts with enhanced valuable performances.

EXPERIMENTAL SECTION

Zwitterionic Polymer. The polyampholyte polymer used in this study was an alternating copolymer, poly(*N*,*N*-diallyl-*N*-hexylamine-*alt*-maleic acid), bearing a long alkyl (hexyl) side chain substituted at the positively charged amine group and the negatively charged maleic acid block. Poly(*N*,*N*-diallyl-*N*-hexylamine-*alt*-maleic acid) (from now on called "copolymer C6") was synthesized according to a procedure reported elsewhere.[26] The structure of the repeating unit of the copolymer is shown in Scheme 1.

Scheme 1. Chemical Structure of the Zwitterionic Form of Polymer, poly(*N*,*N*-diallyl-*N*-hexylamine-*alt*-maleic acid), Used in This Study

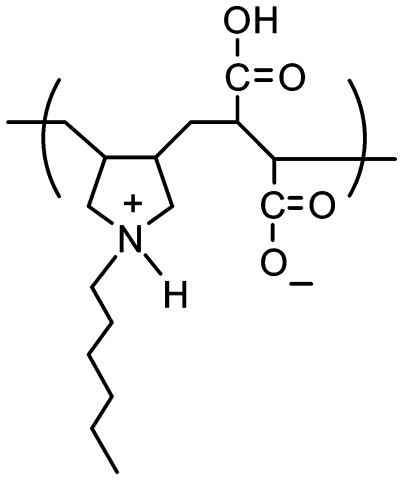

Preparation of Polymer Thin Films. A solution of copolymer C6 (0.05 g/L) was prepared in milli-Q water (Elgastat Maxima system, resistance: 18.2 MΩ) under magnetic stirring for 12 h. The polyampholyte nature of the polymer allows one to obtain completely transparent solutions when stabilized at either high (pH 7.9) or low (pH 2) values of pH as achieved by the addition of aqueous ammonia (0.05 N) or HCl acid (37 wt %, aq), respectively. A drop of the polymer solution (9.5 μL) was then spin-coated at room temperature (22 °C) on a freshly cleaved muscovite mica surface (Agar scientific) at 2000 rpm for 1 min on a commercial spin-coater (Spin 150, Germany).

Preparation of POM−Polymer Hybrid Thin Films. A POM−polymer hybrid solution was prepared by adding an aqueous POM solution (0.1g/L, pH 3.5) to the copolymer C6 solutions (0.05g/L) solubilized at (i) pH 7.9 and (ii) pH 1.8−2, under magnetic stirring for 12 h. The POM:polymer molar ratio in the hybrid was kept at 1:3 in order to meet the charge equivalence between the three times negatively charged POM anion $[PW_{12}O_{40}]^{3-}$ and the single positively charged repeating unit of copolymer C6. The final pH of the hybrid solutions were (i) pH 5.3 and (ii) pH 2. A drop of the hybrid solution was then spin-coated onto a freshly cleaved muscovite mica surface at 2000 rpm for 1 min. The sample was then allowed to dry under ambient conditions overnight.

Atomic Force Microscopy (AFM). AFM experiments were performed using a Nanoscope V multimode AFM (Nano Surfaces Business, Bruker Corporation, Santa Barbara, CA) in the Tapping Mode (TM-AFM) or in the HarmoniX mode under ambient conditions (23 °C and 56% RH). Samples were glued on a magnetic stainless steel disc using a small piece of double-face adhesive tape and mounted on the "J" type piezoelectric scanner. For TM-AFM-etched Si tapping mode cantilever (TESP type, Bruker AFM probes), having a nominal tip radius of an 8 nm curvature was used for imaging at a scan rate of 1 Hz. The tapping engage set point was set to 1 in order to apply minimal engaging force, and images were acquired under "light tapping" conditions in order to minimize sample deformation. The captured raw images were analyzed using Nanoscope (Bruker) for scan analysis and flattened to the zeroth order to remove any underlying surface curvature.

HarmoniX AFM imaging was performed using a special T-shaped torsional cantilever (HMX 10, Bruker probes), with the tip positioned

dx.doi.org/10.1021/la400055t | Langmuir 2013, 29, 4388−4395

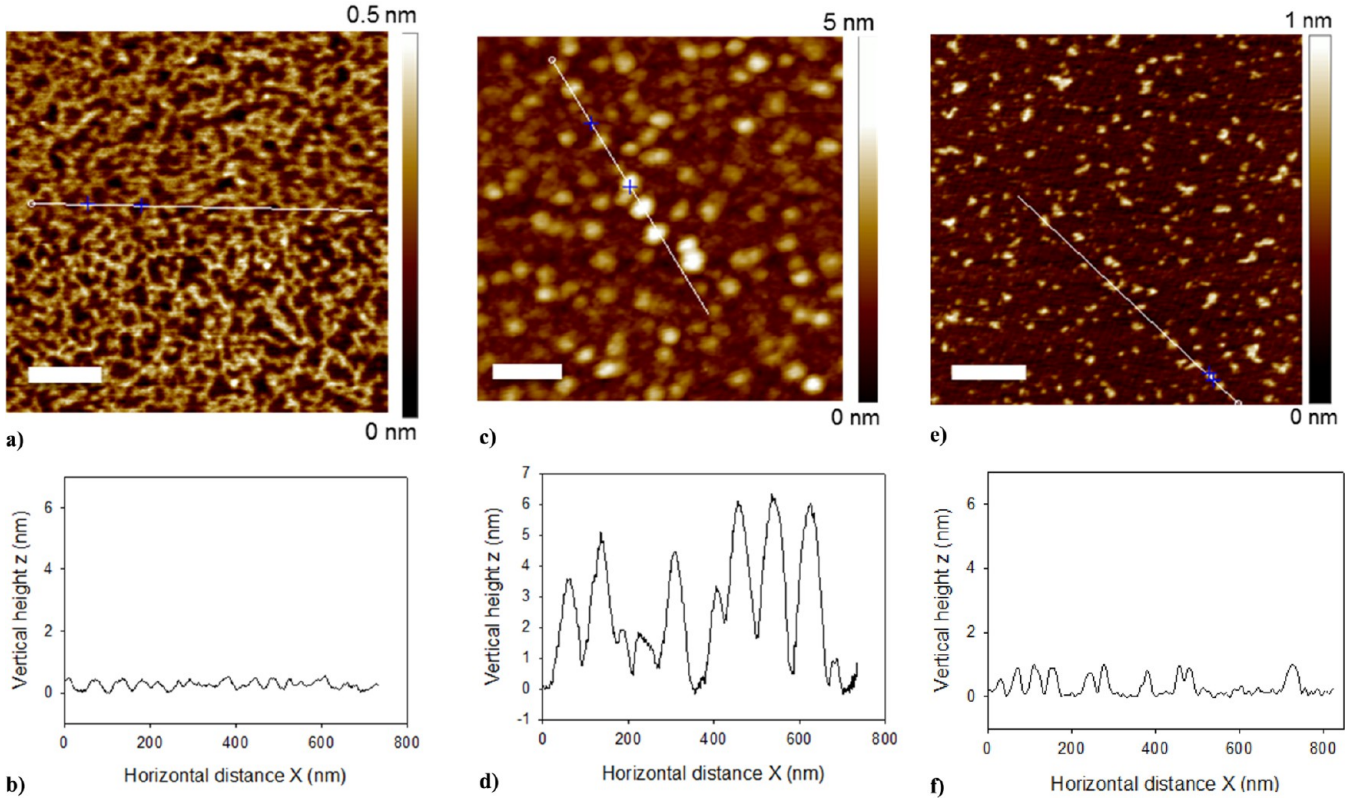

Figure 1. TM-AFM height images of the polyampholyte copolymer spin-coated on the mica surface from solution stabilized at (a) pH 7.9 and (c) pH 2. (b and d) are the corresponding cross-section analysis, respectively. (e) TM-AFM height image of phosphotungstic acid ($H_3PW_{12}O_{40}$) spin-coated on a mica surface and (f) corresponding cross-section analysis. The scale bars are 200 nm.

off-axis of the force sensor. Apart from "classical" AFM data such as height, phase, and amplitude images, HarmoniX mode measures force−distance curves, pixel-by-pixel, generating a 3-dimensional (3D) map of the nanomechanical properties of the surface.[35,36] When tapping on the surface, the offset tip causes torsional motion in addition to the vertical deflection of the cantilever. From the torsional spectrum, force−distance curves are computed at every image pixel. From the maximum positive (or repulsive) force value in the loading part of the force curve, a peak force map is obtained. An adhesion map is obtained from the minimum negative (attractive) force value in the unloading part of the force curve. The map of a local reduced elastic modulus is obtained by fitting the retraction part of the force curve in the constant compliance region using the Derjaguin−Muller−Toporov (DMT) model, assuming a Hertzian contact (spherical tip and flat sample surface). The area between loading and unloading parts of the force curve is used to generate an energy dissipation map between the tip and the sample.[35,36] After determining the flexural and torsional resonant frequencies, the HarmoniX probe was calibrated with the standard method recommended by the manufacturer using a polystyrene (PS)/low density polyethylene (LDPE) blend reference sample. The sample of interest was then mounted on the J-type piezoelectric scanner. For the sample studied, high quality images were obtained when HarmoniX imaging was performed under "low force conditions" (i.e., applying minimum tapping force) achieved by decreasing the drive amplitude and/or increasing the set-point amplitude values. Therefore, the typical values used in this study were 100 mV and 650 mV, respectively.

RESULTS AND DISCUSSION

In the first part, we studied the structure of the spin-coated polyampholyte polymer stabilized under different pH conditions. The objective here was to obtain submonolayer coverage of the polymer films that would allow us to observe polymer chains at their individual length scale. When the initial polymer solution (0.05g/L) was stabilized at a basic pH (pH 7.9), AFM images of the copolymer C6 show fully extended and interconnected chain structures on the mica surface (Figure 1a). The height of the different chain entities measured from the cross-section analysis of the image was 0.6 ± 0.1 nm (Figure 1b). On the other hand, the positively charged polymer stabilized at acidic pH (pH 2) shows globular structures when deposited on the mica surface (Figure 1c). The height of the globular entities measured (4 ± 1 nm) (Figure 1d) was significantly larger than the height of the extended polymer chains, indicating that globular entities mostly consist of aggregates of polymer chains. The globular structure revealed by AFM is also an indication that at pH 2, polymer−polymer interactions were much stronger than polymer−surface interactions. It is important here to consider the surface properties of the freshly cleaved mica surface. It is well-known that a freshly cleaved mica surface, once in contact with a protonated solution, becomes positively charged at the surface due to the migration of potassium ions from the lattice toward the surface.[37] Protons from the solution start interacting with the surface as potassium ions get solvated and leave the surface.[37,38] Thus, at pH 2, since both surface and polymer were positively charged, polymer−polymer interactions are stronger than polymer−surface interactions, resulting in the coil/globular conformation of the polymer. At pH 7.9, the zwitterionic polymer is negatively charged and thus polymer−surface interactions are more favorable at this time, which results in the extended conformation of the C6 copolymer chains on the mica surface as observed by AFM. AFM imaging of spin-coated POM alone was also performed. Figure 1e shows isolated POM entities deposited on the mica surface. The

dx.doi.org/10.1021/la400055t | Langmuir 2013, 29, 4388−4395

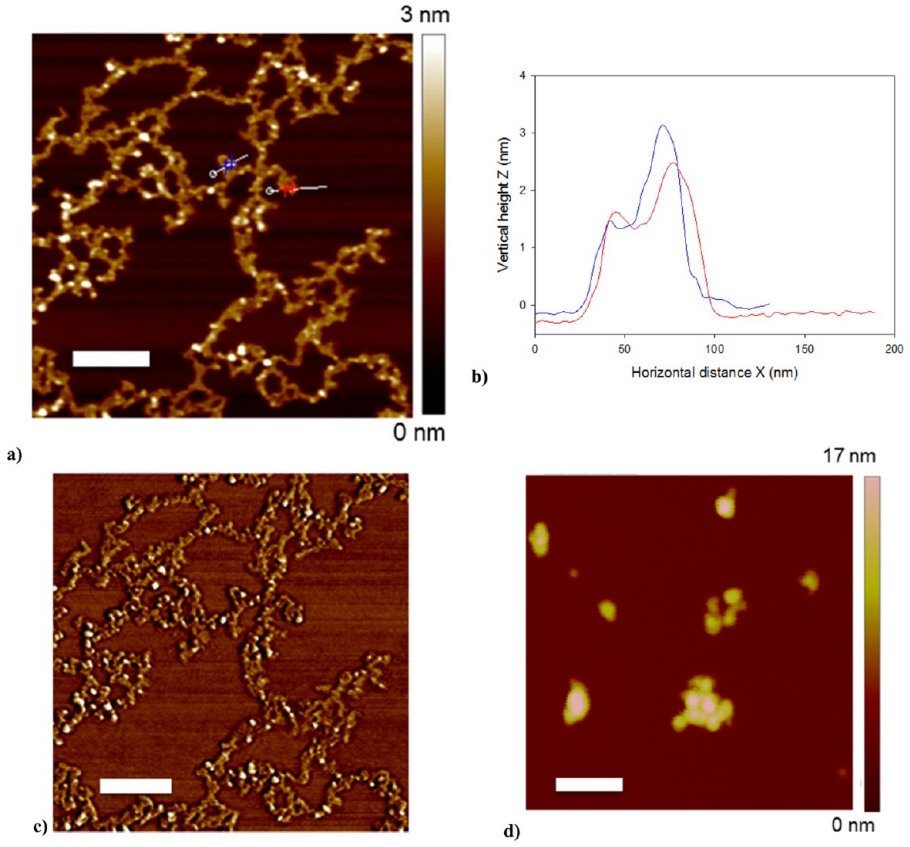

Figure 2. TM-AFM image of POM−polymer hybrid spin-coated on a mica surface. (a) Height image of the POM−polymer hybrid stabilized at pH 5.3. (b) Cross-section showing height analysis of two different POM entities. (c) Corresponding phase image of (a) and (d) height image of the POM−polymer hybrid stabilized at pH 2. The scale bars are 200 nm.

height measured from cross-section analysis of POM entities was 0.9 nm (Figure 1f), which is in close agreement with the theoretical size (diameter ∼1 nm), estimated for the Keggin anion[39,40] $[PW_{12}O_{40}]^{3-}$.

Figure 2a shows the AFM height image of the POM−polymer hybrid, stabilized at pH 5.3 (copolymer C6 solubilized at pH 7.9 + $H_3PW_{12}O_{40}$). The decrease in pH of the hybrid solution, when compared to the initial polymer solution (pH 7.9), is due to the addition of POM, which is known to be a strong proton donor. The hybrid material, deposited on the mica surface, forms long and extended chain structures with well-defined and bright spherical entities appearing at different sites along the polymer chains. The height measured on these bright spherical entities varied from 2.8 ± 0.1 to 3.3 ± 0.1 nm, whereas that measured on the extended chain structures was 1.7 ± 0.1 nm (Figure 2b). The difference in height (with respect to polymer chains) was ∼1 nm on one spherical entity while ∼1.6 nm on the other, suggesting that different kinds of POM molecules may be attached to the polymer chains. It has been reported that the Keggin type $H_3PW_{12}O_{40}$ would dissociate to P_2W_{21}, PW_{11}, and P_2W_{18} species at pH 5.4.[41] However, some other studies reported a greater stability of Keggin POM in the larger pH range (5−7), when they are immobilized on a substrate through hybridization,[42] which is very similar to what happens in our hybrid stabilized at pH 5.3. Moreover, in Figure 2a, we never observed any isolated POM species laying outside of the polymer matrix. This shows that all the negatively charged POM species are interacting with the polymer. Although from Figure 2b, it would be difficult to associate the size of POM as observed from AFM to the known structures of POM, stable at a pH of 5.3. For instance, objects of ∼1 nm high could be either (lacunary) Keggin or "two P containing POM" (e.g., Dawson POM laying flat). Similarly, objects of ∼1.5 nm high might be Dawson POM standing vertical or superposing (lacunary) Keggin. The contrast between POM entities and the polymer chains were better resolved in AFM phase images (Figure 2c), where POM appears as well-defined bright spheres attached to darker polymer chains. TM-phase images, which were obtained by simultaneously monitoring the phase shift between the drive signal to the cantilever and its response, are known to be sensitive to the energy dissipation at the tip−surface contact. In specific conditions, hard materials appear as bright regions due to a larger positive phase shift, while softer materials appear as darker regions due to a smaller phase shift.[43] Thus, from the AFM height and phase images of the hybrid system, the bright spherical entities in the phase image can be associated with hard POM that are electrostatically attached to the positively charged sites along the polymer chains.

On the other hand, the POM−polymer hybrid stabilized at acidic pH (pH 2) forms isolated 12 ± 2 nm high aggregates on the mica surface (Figure 2d). It is interesting to note that the height of the aggregates was larger when compared to that of the polymer alone at pH 2 (Figure 1c), suggesting that the hybrid aggregates are not just the polymer alone but the result of a hybrid assembly of POM and polymer matrix. As the polymer is positively charged at pH 2, it readily interacts with the negatively charged POM anions through electrostatic interactions. Due to the large size and charge of POM anions, it is most likely that the positively charged polymer chains

dx.doi.org/10.1021/la400055t | *Langmuir* 2013, 29, 4388−4395

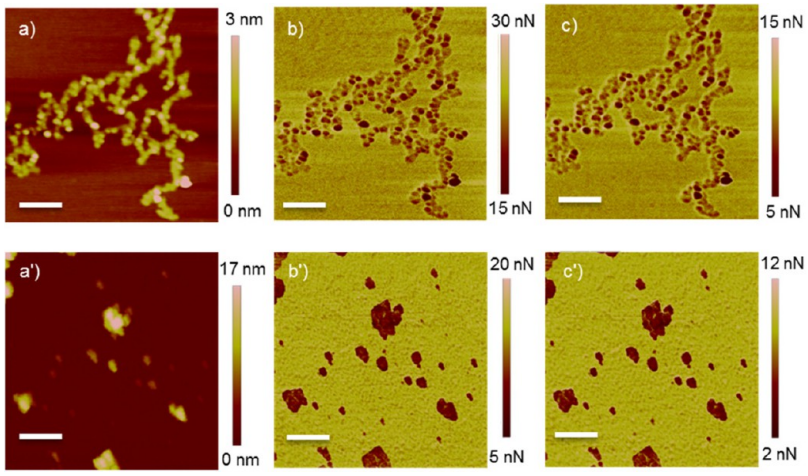

Figure 3. HarmoniX-AFM height, peak force, and adhesion force maps of the POM−polymer hybrid stabilized at pH 5.3 (a−c, respectively) and at pH 2 (a′−c′, respectively). The scale bars are 200 nm.

envelop POM entities to form encapsulated species. Earlier studies have reported the formation of such encapsulated species of POM anions, driven by electrostatic interactions with cationic surfactant molecules such as dimethyldioctadecylammonium bromide (DODA-Br).[24,44]

AFM HarmoniX Imaging of the Hybrid. As thin films of polymers and the hybrid material were used in this study, low tapping force conditions (amplitude set point = 700 mV and drive amplitude = 100 mV) were used in HarmoniX imaging to minimize the influence of the substrate on the measurements and to enable imaging of the sample surface with high spatial resolution. High resolution data were indeed obtained in the peak and adhesion force channels, when compared to dissipation and DMT-modulus channels and, hence, are discussed in detail for quantitative comparison. The low resolution of modulus maps is due to the well-known substrate-effect on supported ultrathin films,[45−47] as is the case in our system.

Figure 3 shows the HarmoniX images of the POM−polymer hybrid material stabilized at two different pH values. The height images were similar to those acquired in classical AFM. POM-decorated polymer chains were observed when the hybrid material was stabilized at pH 5.3 (Figure 3, panels a−c). POM entities attached to the polymer chains were observed with the highest spatial resolution (appearing as distinct dark spheres) in the peak force (F_p) and adhesion force (F_{adh}) maps (Figure 3, panels b and c, respectively). Peak force is directly related to the sample stiffness, while adhesion force between the tip and the sample is a result of several interaction forces, including van der Waals (F_{vdw}), capillary (F_{cap}), electrostatic (F_e), and chemical bonding forces (F_b).[48] Under ambient conditions (22 °C, 56% relative humidity), contribution from F_{cap}, which is due to a condensed thin layer of water molecules on hydrophilic surfaces,[49] is expected to be predominant on the POM surface, which is water-soluble and hydrophilic. In the case of the POM−polymer hybrid stabilized under acidic condition (pH 2), the hybrid entities appear as isolated aggregates on the mica surface (Figure 3, panels a′−c′). Once again, sharp contrasts between features were observed in peak and adhesion force maps, when compared to the topography image alone.

For comparison, height, peak, and adhesion force maps of pure samples [i.e., POM only (panels a−c)] and copolymer C6 samples stabilized at pH 7.9 (panels a′−c′) and pH 2 (panels a″−c″) are shown in Figure S1 of the Supporting Information. In the case of the copolymer stabilized at pH 7.9, the contrast between features observed in the peak and adhesion force maps were not well-resolved (Figure S1, panels b′ and c′ of the Supporting Information). This is attributed to the substrate-effect when the tip indents on subnanometer thick (0.6 nm) soft polymer chains. However, it is interesting here to note that the values of peak and adhesion forces measured on the POM sample alone were similar to those measured on the well-defined spherical entities observed on the POM−polymer stabilized at pH 5.3. Also, similar values of peak and adhesion forces were recorded for the copolymer as well as for the POM−polymer hybrid, stabilized at pH 2 (see Table 1). These measurements, for the first time, provide solid evidence that POM entities were arranged on the polymer chains when the hybrid material was stabilized at pH 5.3, while at pH 2, the hybrid material consists of POM entities encapsulated by the polymer chains.

Table 1. Comparison of Quantitative Data Obtained From HarmoniX AFM Imaging

	height (nm)	peak force (nN)	adhesion (nN)
POM ($H_3PW_{12}O_{40}$)	0.9	25	7
copolymer C6 (pH 2)	3.7	7	3.5
hybrid (Copolymer C6 + POM) at pH 5.3	2.7	18.5	6
hybrid (Copolymer C6 +POM) at pH 2	11.5	4.8	2.5

From the adhesion force maps, statistical analysis of distances between pairs of POM entities (n = 40) on the POM−polymer hybrid stabilized at pH 5.3 (Figure 4a), as well as on the POM samples alone (Figure 4b), were performed using the software R-2.15.2[50] with the package vioplot.[51] The data are represented as violin plots that combine the basic statistics summary of the box plot and the density trace (or smoothed histogram) into a single plot.[52] Figure 4c compares the violin plots of the POM−polymer hybrid and POM samples alone, illustrating the distribution of interparticle distances, as well as the median (white dot). It can be observed that the median values of interparticle distances were 40 and 180 nm in the case of the POM−polymer hybrid and the POM sample alone, respec-

dx.doi.org/10.1021/la400055t | Langmuir 2013, 29, 4388−4395

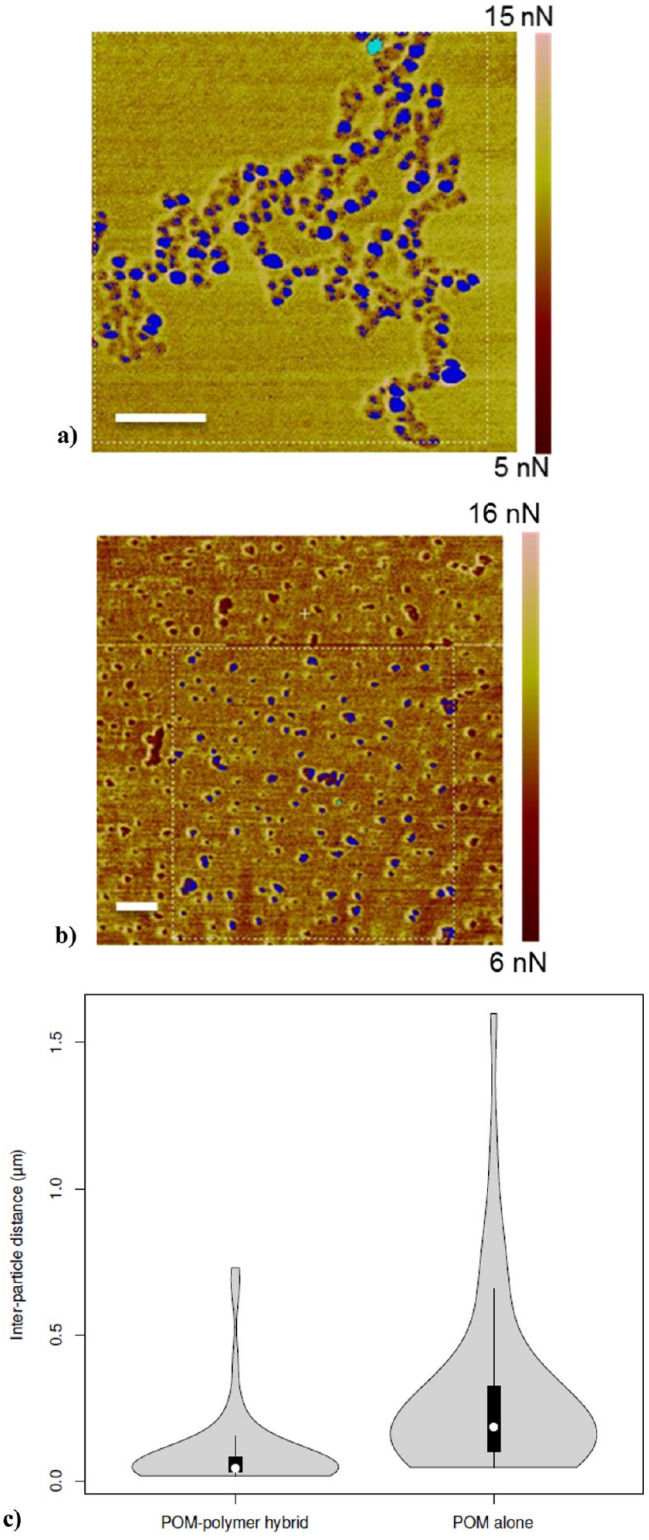

Figure 4. Distance measurements between adjacent POM entities from the AFM HarmoniX adhesion force maps of (a) POM–polymer hybrid stabilized at pH 5.3 and (b) $H_3PW_{12}O_{40}$ POM. The scale bars are 200 nm. (c) Corresponding violin plots illustrate the median value of inter-POM distances (white spot) at 40 and 180 nm for the POM–polymer hybrid and the POM sample, respectively. Black boxes are the quartiles, and the solid lines are the range of points laying within 1.5 times the interquartile range of the box. The narrow distribution of density trace for the POM–polymer hybrid signifies a high level of ordering of POM entities along the polymer chains.

tively. Further, narrow distribution of the density trace was obtained for the POM–polymer hybrid, when compared to the broad distribution in the POM sample alone. This is consistent with an ordered arrangement of POM entities along the polymer chains. The ordering of POM results from its interaction with the charge sites, which themselves appear regularly along the chain (alteration of monomers bearing a positive charge with those bearing a negative charge).

CONCLUSION

We report here an AFM study on the supramolecular assembly of an organic–inorganic heterogeneous hybrid catalyst formed from a poly(ampholyte) polymer, poly(*N*,*N*-diallyl-*N*-hexylamine-*alt*-maleic acid), together with phosphotungstic acid ($H_3PW_{12}O_{40}$). The initial conformation of the polyampholyte host polymer on the surface was found to be dependent on the pH of the stabilizing solution. When deposited on the mica surface, poly(*N*,*N*-diallyl-*N*-hexylamine-*alt*-maleic acid) forms long and extended polymer chains (height 0.6 nm) under basic conditions (pH 7.9), while under acidic conditions (pH 2), nanoglobules (height 4 nm) were formed. We demonstrate that the supramolecular architecture of the organic–inorganic hybrid formed through electrostatic interactions could in turn be tuned by the nature and the quantity of the charges present on the polyampholyte polymer stabilized under the different pH conditions. At acidic pH, POM anions were encapsulated by the positively charged polymer chains to form encapsulated clusters. On the other hand, at a more basic pH (5.3), POM-decorated extended polymer chains were observed by AFM. These supramolecular hybrid structures are confirmed by measuring the nanomechanical properties of the polymer and of the POM phases in the hybrid films using HarmoniX AFM imaging. Peak and adhesion force maps allow one to quantitatively distinguish the POM and polymer phases in the hybrid, with a remarkably high spatial resolution. Distance measured between the adjacent hybridized POM entities revealed narrow distribution, signifying an ordered arrangement of POM entities along the polymer chains. The developed strategies here evidence the parameters that will allow one to tailor the supramolecular structures of POM-based organic–inorganic heterogeneous hybrid catalysts and thus offer promising future applications, where POM should be (at wish) either encapsulated to form molecular reaction vessels or isolated on a support surface via their long-range order, dictated by the polymer matrix. These two situations might indeed bring totally different catalytic behaviors that would be highly valuable to switch from one to another.

ASSOCIATED CONTENT

Supporting Information

HarmoniX AFM height, peak force, and adhesion force maps of phosphotungstic acid ($H_3PW_{12}O_{40}$) and copolymer C6 stabilized at pH 7.9 and pH 2. This material is available free of charge via the Internet at http://pubs.acs.org.

AUTHOR INFORMATION

Corresponding Author

*G.R.: e-mail, gijo.raj@uclouvain.be. E.M.G.: e-mail, eric.gaigneaux@uclouvain.be. Tel: ++32/10/473665. Fax: ++32/10/473649.

Notes

The authors declare no competing financial interest.

dx.doi.org/10.1021/la400055t | *Langmuir* 2013, 29, 4388–4395

■ ACKNOWLEDGMENTS

The authors are grateful for the financial support from the "Communauté Française de Belgique" through the ARC programme (Grant 08/13-009) and Fonds National de la Recherche Scientifique (FRS-FNRS) Belgium for the acquisition of the AFM. We would like to thank Ronald Lasselin for the synthesis of polymers, Dr. K. Mc Evoy for MATLAB programming, and S. Derclaye for AFM technical assistance.

■ REFERENCES

(1) Katsoulis, D. E. A Survey of Applications of Polyoxometalates. *Chem. Rev.* **1998**, *98*, 359−388.
(2) Long, D.-L.; Burkholder, E.; Cronin, L. Polyoxometalate Clusters, Nanostructures and Materials: From Self Assembly to Designer Materials and Devices. *Chem. Soc. Rev.* **2007**, *36*, 105−121.
(3) Cronin, L.; Muller, A. From Serendipity to Design of Polyoxometalates at the Nanoscale, Aesthetic Beauty, and Applications. *Chem. Soc. Rev.* **2012**, *41*, 7333−7334.
(4) Compain, J.-D.; Mialane, P.; Dolbecq, A.; Mbomekallé, I. M.; Marrot, J.; Sécheresse, F.; Rivière, E.; Rogez, G.; Wernsdorfer, W. Iron Polyoxometalate Single-Molecule Magnets. *Angew. Chem., Int. Ed.* **2009**, *48*, 3077−3081.
(5) Fan, D.; Hao, J. Magnetic Aligned Vesicles. *J. Colloid Interface Sci.* **2010**, *342*, 43−48.
(6) Luban, M.; Borsa, F.; Budko, S.; Canfield, P.; Jun, S.; Jung, J. K.; Kögerler, P.; Mentrup, D.; Müller, A.; Modler, R.; et al. Heisenberg Spin Triangles in {V-6}-Type Magnetic Molecules: Experiment and Theory. *Phys. Rev. B: Condens. Matter Mater. Phys.* **2002**, *66*, 054407.
(7) Chaidogiannos, G.; Velessiotis, D.; Argitis, P.; Koutsolelos, P.; Diakoumakos, C. D.; Tsamakis, D.; Glezos, N. Tunneling and Negative Resistance Effects for Composite Materials Containing Polyoxometalate Molecules. *Microelectron. Eng.* **2004**, *73*−*74*, 746−751.
(8) Liu, S.; Möhwald, H.; Volkmer, D.; Kurth, D. G. Polyoxometalate-Based Electro- and Photochromic Dual-Mode Devices. *Langmuir* **2006**, *22*, 1949−1951.
(9) Zhang, T.; Liu, S.; Kurth, D. G.; Faul, C. F. J. Organized Nanostructured Complexes of Polyoxometalates and Surfactants that Exhibit Photoluminescence and Electrochromism. *Adv. Funct. Mater.* **2009**, *19*, 642−652.
(10) Rhule, J. T.; Hill, C. L.; Judd, D. A.; Schinazi, R. F. Polyoxometalates in Medicine. *Chem. Rev.* **1998**, *98*, 327−358.
(11) Kawasaki, N.; Wang, H.; Nakanishi, R.; Hamanaka, S.; Kitaura, R.; Shinohara, H.; Yokoyama, T.; Yoshikawa, H.; Awaga, K. Nanohybridization of Polyoxometalate Clusters and Single-Wall Carbon Nanotubes: Applications in Molecular Cluster Batteries. *Angew. Chem., Int. Ed.* **2011**, *123*, 3533−3536.
(12) Guo, Y.; Hu, C. Heterogeneous Photocatalysis by Solid Polyoxometalates. *J. Mol. Catal. A: Chem.* **2007**, *262*, 136−148.
(13) Keita, B.; Abdeljalil, E.; Nadjo, L.; Contant, R.; Belghiche, R. Cooperativity of Copper and Molybdenum Centers in Polyoxometalate-Based Electrocatalysts: Cyclic Voltammetry, EQCM, and AFM Characterization. *Langmuir* **2006**, *22*, 10416−10425.
(14) Mizuno, N.; Misono, M. Heteropolyanions in Catalysis. *J. Mol. Catal.* **1994**, *86*, 319−342.
(15) Noro, S.-i.; Tsunashima, R.; Kamiya, Y.; Uemura, K.; Kita, H.; Cronin, L.; Akutagawa, T.; Nakamura, T. Adsorption and Catalytic Properties of the Inner Nanospace of a Gigantic Ring-Shaped Polyoxometalate Cluster. *Angew. Chem., Int. Ed.* **2009**, *121*, 8859−8862.
(16) Li, G.; Ding, Y.; Wang, J.; Wang, X.; Suo, J. New Progress of Keggin and Wells-Dawson Type Polyoxometalates Catalyze Acid and Oxidative Reactions. *J. Mol. Catal. A: Chem* **2007**, *262*, 67−76.
(17) Qi, W.; Li, H.; Wu, L. Stable Photochromism and Controllable Reduction Properties of Surfactant-Encapsulated Polyoxometalate/Silica Hybrid Films. *J. Phys. Chem. B* **2008**, *112*, 8257−8263.
(18) Zhang, Z.; Zhao, W.; Ma, B.; Ding, Y. The Epoxidation of Olefins Catalyzed by a New Heterogeneous Polyoxometalate-Based Catalyst with Hydrogen Peroxide. *Catal. Commun.* **2010**, *12*, 318−322.
(19) Musumeci, C.; Luzio, A.; Pradeep, C. P.; Miras, H. N.; Rosnes, M. H.; Song, Y.-F.; Long, D.-L.; Cronin, L.; Pignataro, B. Programmable Surface Architectures Derived from Hybrid Polyoxometalate-Based Clusters. *J. Phys. Chem. C* **2011**, *115*, 4446−4455.
(20) Song, Y.-F.; McMillan, N.; Long, D.-L.; Thiel, J.; Ding, Y.; Chen, H.; Gadegaard, N.; Cronin, L. Design of Hydrophobic Polyoxometalate Hybrid Assemblies Beyond Surfactant Encapsulation. *Chem.—Eur. J.* **2008**, *14*, 2349−2354.
(21) Yin, P.; Li, D.; Liu, T. Solution Behaviors and Self-Assembly of Polyoxometalates As Models of Macroions and Amphiphilic Polyoxometalate-Organic Hybrids As Novel Surfactants. *Chem. Soc. Rev.* **2012**, *41*, 7368−7383.
(22) Bu, W.; Li, H.; Sun, H.; Yin, S.; Wu, L. Polyoxometalate-Based Vesicle and Its Honeycomb Architectures on Solid Surfaces. *J. Am. Chem. Soc.* **2005**, *127*, 8016−8017.
(23) Ohmatsu, K.; Ito, M.; Kunieda, T.; Ooi, T. Ion-Paired Chiral Ligands for Asymmetric Palladium Catalysis. *Nat. Chem.* **2012**, *4*, 473−477.
(24) Wu, P.; Volkmer, D.; Bredenkotter, B.; Kurth, D. G.; Rabe, J. P. Isolated and Linear Arrays of Surfactant-Encapsulated Polyoxometalate Clusters on Graphite. *Langmuir* **2008**, *24*, 2767−2771.
(25) Bao, Y.-Y.; Bi, L.-H.; Wu, L.-X.; Mal, S. S.; Kortz, U. Preparation and Characterization of Langmuir−Blodgett Films of Wheel-Shaped Cu-20 Tungstophosphate and DODA by Two Different Strategies. *Langmuir* **2009**, *25*, 13000−13006.
(26) Rullens, F.; Devillers, M.; Laschewsky, A. New Regular, Amphiphilic Poly(ampholyte)s: Synthesis and Characterization. *Macromol. Chem. Phys.* **2004**, *205*, 1155−1166.
(27) Rullens, F.; Devillers, M.; Laschewsky, A. Preparation of Simple and Mixed Nickel and Cobalt Molybdates Using Hybrid Precursors Made from an Ordered Polymer Matrix and Inorganic Salts. *J. Mater. Chem.* **2004**, *14*, 3421−3426.
(28) Farin, B.; Swalus, C.; Devillers, M.; Gaigneaux, E. M. NiMoO4 Preparation from Polyampholytic Hybrid Precursors: Benefiting of the Memory Effect in the Oxidative Dehydrogenation of Propane. *Catal. Today* **2013**, *203*, 24−31.
(29) Kukovecz, A.; Balogi, Z.; Konya, Z.; Toba, M.; Lentz, P.; Niwa, S. I.; Mizukami, F.; Molnar, A.; Nagy, J. B.; Kiricsi, I. Synthesis, Characterisation and Catalytic Applications of Sol-Gel Derived Silia-Phosphotungstic Acid Composites. *Appl. Catal., A* **2002**, *228*, 83−94.
(30) Nandhini, K. U.; Arabindoo, B.; Palanichamy, M.; Murugesan, V. Al-MCM-41 Supported Phosphotungstic Acid: Application to Symmetrical and Unsymmetrical Ring Opening of Succinic Anhydride. *J. Mol. Catal. A: Chem.* **2006**, *243*, 183−193.
(31) Kim, J.-D.; Honma, I. Synthesis and Proton Conducting Properties of Zirconia Bridged Hydrocarbon/Phosphotungstic Acid Hybrid Materials. *Electrochim. Acta* **2004**, *49*, 3179−3183.
(32) Feng, W.; Ding, Y.; Liu, Y.; Lu, R. The Photochromic Process of Polyoxometalate-Based Nanocomposite Thin Film by in Situ AFM and Spectroscopy. *Mater. Chem. Phys.* **2006**, *98*, 347−352.
(33) Aradhya, S. V.; Frei, M.; Hybertsen, M. S.; Venkataraman, L. Van der Waals Interactions at Metal/Organic Interfaces at the Single-Molecule Level. *Nat. Mater.* **2012**, *11*, 872−876.
(34) Grzelczak, M.; Vermant, J.; Furst, E. M.; Liz-Marzan, L. M. Directed Self-Assembly of Nanoparticles. *ACS Nano* **2010**, *4*, 3591−3605.
(35) Sahin, O.; Quate, C. F.; Solgaard, O.; Atalar, A. Resonant Harmonic Response in Tapping-Mode Atomic Force Microscopy. *Phy. Rev. B* **2004**, *69*, 165416.
(36) Sahin, O.; Magonov, S.; Su, C.; Quate, C. F.; Solgaard, O. An Atomic Force Microscope Tip Designed to Measure Time-Varying Nanomechanical Forces. *Nat. Nanotechnol.* **2007**, *2*, 507−514.
(37) Sides, P. J.; Faruqui, D.; Gellman, A. J. Dynamics of Charging of Muscovite Mica: Measurement and Modeling. *Langmuir* **2009**, *25*, 1475−1481.

(38) Maslova, M. V.; Gerasimova, L. G.; Forsling, W. Surface Properties of Cleaved Mica. *Colloid J.* **2004**, *66*, 322−328.
(39) Kaba, M. S.; Song, I. K.; Duncan, D. C.; Hill, C. L.; Barteau, M. A. Molecular Shapes, Orientation, and Packing of Polyoxometalate Arrays Imaged by Scanning Tunneling Microscopy. *Inorg. Chem.* **1998**, *37*, 398−406.
(40) Brown, G. M.; Noe-Spirlet, M.-R.; Busing, W. R.; Levy, H. A. Dodecatungstophosphoric Acid Hexahydrate, $(H_5O_2^+)_3(PW_{12}O_{40}^{3-})$. The True Structure of Keggin'S Pentahydrate' from Single-Crystal X-ray and Neutron Diffraction Data. *Acta Crystallogr., Sect. B* **1977**, *33*, 1038−1046.
(41) Zhu, Z.; Tain, R.; Rhodes, C. A Study of the Decomposition Behaviour of 12-Tungstophosphate Heteropolyacid in Solution. *Can. J. Chem.* **2003**, *81*, 1044−1050.
(42) Tang, Z.; Liu, S.; Wang, E.; Dong, S.; Wang, E. Preparation, Structures, and Electrochemistry of a New Polyoxometalate-Based Organic/Inorganic Film on Carbon Surfaces. *Langmuir* **2000**, *16*, 5806−5813.
(43) James, P. J.; Antognozzi, M.; Tamayo, J.; McMaster, T. J.; Newton, J. M.; Miles, M. J. Interpretation of Contrast in Tapping Mode AFM and Shear Force Microscopy. A Study of Nafion. *Langmuir* **2001**, *17*, 349−360.
(44) Akutagawa, T.; Jin, R.; Tunashima, R.; Noro, S.-i.; Cronin, L.; Nakamura, T. Nanoscale Assemblies of Gigantic Molecular $\{Mo_{154}\}$-Rings: $(Dimethyldioctadecylammonium)_{20}[Mo_{154}O_{462}H_8(H2O)_{70}]$. *Langmuir* **2008**, *24*, 231−238.
(45) Cappella, B.; Silbernagl, D. Nanomechanical Properties of Polymer Thin Films Measured by Force Distance Curves. *Thin Solid Films* **2008**, *516*, 1952−1960.
(46) Domke, J.; Radmacher, M. Measuring the Elastic Properties of Thin Polymer Films with the Atomic Force Microscope. *Langmuir* **1998**, *14*, 3320−3325.
(47) Silbernagl, D.; Sturm, H.; Cappella, B. Influence of Film-Substrate Adhesion on the Mechanical Properties of Thin Polymer Films. *Langmuir* **2009**, *25*, 5091−5097.
(48) Butt, H.-J. r.; Cappella, B.; Kappl, M. Force Measurements with the Atomic Force Microscope: Technique, Interpretation and Applications. *Surf. Sci. Rep.* **2005**, *59*, 1−152.
(49) Xiao, X.; Qian, L. Investigation of Humidity-Dependent Capillary Force. *Langmuir* **2000**, *16*, 8153−8158.
(50) R Foundation for Statistical Computing. *R: A Language and Environment for Statistical Computing*. R Core Team: Vienna, Austria,3-900051-07-0 (http://www.R-project.org/).
(51) Adler, D. *R package Vioplot: Violin plot*, version 0.2; 2005 (http://wsopuppenkiste.wiso.uni-goettingen.de/~dadler).
(52) Hintze, J. L.; Nelson, R. D. Violin Plots: A Box Plot-Density Trace Synergism. *Am. Stat.* **1998**, *52*, 181−184.